JCI insight

CXCL13-producing T_{FH} cells link immune suppression and adaptive memory in human breast cancer

Chunyan Gu-Trantien, … , Denis Larsimont, Karen Willard-Gallo

JCI Insight. 2017;2(11):e91487. https://doi.org/10.1172/jci.insight.91487.

Research Article | Immunology | Oncology

T follicular helper cells (T_{FH} cells) are important regulators of antigen-specific B cell responses. The B cell chemoattractant CXCL13 has recently been linked with T_{FH} cell infiltration and improved survival in human cancer. Although human T_{FH} cells can produce CXCL13, their immune functions are currently unknown. This study presents data from human breast cancer, advocating a role for tumor-infiltrating CXCL13-producing ($CXCR5^{-}$) T_{FH} cells, here named $T_{FH}X13$ cells, in promoting local memory B cell differentiation. $T_{FH}X13$ cells potentially trigger tertiary lymphoid structure formation and thereby generate germinal center B cell responses at the tumor site. Follicular DCs are not potent CXCL13 producers in breast tumor tissues. We used the T_{FH} cell markers PD-1 and ICOS to identify distinct effector and regulatory $CD4^{+}$ T cell subpopulations in breast tumors. $T_{FH}X13$ cells are an important component of the $PD\text{-}1^{hi}ICOS^{int}$ effector subpopulation and coexpanded with $PD\text{-}1^{hi}ICOS^{int}FOXP3^{hi}$ Tregs. IL2 deprivation induces CXCL13 expression in vitro with a synergistic effect from TGFβ1, providing insight into $T_{FH}X13$ cell differentiation in response to Treg accumulation, similar to conventional T_{FH} cell responses. Our data suggest that human $T_{FH}X13$ cell differentiation may be a key factor in converting Treg-mediated immune suppression to de novo activation of adaptive antitumor humoral responses in the chronic inflammatory breast cancer microenvironment.

Find the latest version:

https://jci.me/91487/pdf



JCI insight

RESEARCH ARTICLE

CXCL13-producing T_{FH} cells link immune suppression and adaptive memory in human breast cancer

Chunyan Gu-Trantien,[1] Edoardo Migliori,[1] Laurence Buisseret,[1,2] Alexandre de Wind,[3] Sylvain Brohée,[2] Soizic Garaud,[1] Grégory Noël,[1] Luan Dang C.V.,[4] Jean-Nicolas Lodewyckx,[1] Céline Naveaux,[1] Hugues Duvillier,[5] Stanislas Goriely,[6] Denis Larsimont,[3] and Karen Willard-Gallo[1]

[1]Molecular Immunology Unit, [2]Breast Cancer Translational Research Laboratory, [3]Anatomical Pathology, [4]Hematology, [5]Flow Cytometry Core Facility, Institut Jules Bordet, [6]Welbio and Institute for Medical Immunology, Université Libre de Bruxelles, Brussels, Belgium.

T follicular helper cells (T_{FH} cells) are important regulators of antigen-specific B cell responses. The B cell chemoattractant CXCL13 has recently been linked with T_{FH} cell infiltration and improved survival in human cancer. Although human T_{FH} cells can produce CXCL13, their immune functions are currently unknown. This study presents data from human breast cancer, advocating a role for tumor-infiltrating CXCL13-producing ($CXCR5^-$) T_{FH} cells, here named $T_{FH}X13$ cells, in promoting local memory B cell differentiation. $T_{FH}X13$ cells potentially trigger tertiary lymphoid structure formation and thereby generate germinal center B cell responses at the tumor site. Follicular DCs are not potent CXCL13 producers in breast tumor tissues. We used the T_{FH} cell markers PD-1 and ICOS to identify distinct effector and regulatory $CD4^+$ T cell subpopulations in breast tumors. $T_{FH}X13$ cells are an important component of the $PD\text{-}1^{hi}ICOS^{int}$ effector subpopulation and coexpanded with $PD\text{-}1^{hi}ICOS^{int}FOXP3^{hi}$ Tregs. IL2 deprivation induces CXCL13 expression in vitro with a synergistic effect from TGFβ1, providing insight into $T_{FH}X13$ cell differentiation in response to Treg accumulation, similar to conventional T_{FH} cell responses. Our data suggest that human $T_{FH}X13$ cell differentiation may be a key factor in converting Treg-mediated immune suppression to de novo activation of adaptive antitumor humoral responses in the chronic inflammatory breast cancer microenvironment.

Introduction

T follicular helper cells (T_{FH} cells) are a functionally distinct $CD4^+$ T cell subpopulation that differentiate in secondary lymphoid organ germinal centers (GC) and play critical roles generating and maintaining Ab-producing and memory B cells (1). As an important component of the immune response to viral infection, T_{FH} cells have a contributory role in autoimmunity (2). Recent analysis of human blood identified 3 major functional subsets ($T_{FH}1$, $T_{FH}2$, and $T_{FH}17$) (3), with specific T_{FH} subsets correlated with broad neutralizing anti-viral Ab or auto-Ab (4).

Studies of T_{FH} cells in cancer are fairly recent. We identified them in human breast cancer (BC) as residents of peritumoral tertiary lymphoid structures (TLS) and associated their presence with CXCL13 expression (5). In colorectal cancer, CXCL13 was detected in both T cells and tumor cells with a *CXCL13* deletion linked to fewer infiltrating T_{FH} and B cells (6). Both studies show that high *CXCL13* gene expression is a strong predictor for better patient outcome; however, discrepancies in human and animal model studies concerning pro- or antitumor activities by CXCL13 suggest that its role in cancer merits further investigation.

Known as a potent B cell chemoattractant, CXCL13 is a key factor for initiating secondary lymphoid organ development (7). It is required for early recruitment of lymphoid tissue inducer cells and functions upstream of other early signals, including the lymphotoxin-β receptor (8). De novo TLS formation in chronically inflamed tissues has been correlated with allograft rejection, autoimmune disease progression (9), and improved cancer outcomes (10). Influenza-induced TLS in the lung (but not nearby secondary lymphoid organs) and the subsequent generation of resident memory B cells were responsible for limiting virus escape after infection (11). In some tissues, in vivo TLS formation can be initiated by mature

Conflict of interest: The authors have declared that no conflict of interest exists.

Submitted: November 7, 2016
Accepted: April 25, 2017
Published: June 2, 2017

Reference information:
JCI Insight. 2017;2(11):e91487. https://doi.org/10.1172/jci.insight.91487.

$CD3^+CD4^+$ T cells in the absence of lymphoid tissue inducer cells (12). CXCL13 has been specifically associated with TLS development. Ectopic CXCL13 expression is sufficient for recruiting B cells and inducing TLS formation in nonlymphoid tissues (13), while inhibiting CXCL13 disrupts their formation (14). In murine secondary lymphoid organs, CXCL13 is principally produced by stromal cells resident in B cell follicles, including follicular DCs (FDC) (15) and marginal reticular cells (the latter absent in TLS) (16). Contrary to mice (17, 18), in humans there is evidence that GC T_{FH} cells can be potent CXCL13 producers (19–22), although their physiological role is unclear.

GC T_{FH} cells coexpress the highest levels of surface PD-1, CXCR5 (the CXCL13 receptor), and ICOS, with BCL6 as their distinguishing transcription factor and IL21 as their characteristic cytokine (23). Surface CD200, a designated T_{FH} marker, also increases in some inflammatory conditions (24). We identified $PD\text{-}1^{hi}CD200^{hi}CD4^+$ tumor-infiltrating lymphocytes (TIL) in human BC specifically expressing CXCL13 (5, 25), but curiously, the majority were $CXCR5^-$ cells located both in TLS containing a GC (TLS/GC) and the tumor bed. $CXCR5^-CXCL13^+CD4^+$ T cells have also been detected in rheumatoid synovitis from patients but were not viewed as T_{FH} cells because of their CXCR5 negativity (26, 27).

A recent study found that TGFβ1 is a key CXCL13-inducing factor in human blood $CD4^+$ T cells, triggering $CXCR5^+$ T cell and B cell migration (28). The work reported here and our other recent experiments (data not shown) found that IL2 deprivation is critical for CXCL13 induction, with TGFβ1 providing a synergistic signal only. IL2 has previously been found to negatively regulate T_{FH} cell differentiation (29), while IL2 consumption by Tregs was shown to be essential for murine T_{FH} development and the subsequent GC response (30). This data suggest that the balance between these $CD4^+$ subpopulations is influenced by their surrounding microenvironment.

The present study extends our previous findings (5) by showing $CD4^+$ (and some $CD8^+$) TIL, but not FDC, are major CXCL13 producers in human BC. The phenotypic characteristics of these $CXCL13^+CD4^+$ TIL, their relative importance within the $CD4^+$ T cell compartment, and their role(s) in BC-associated TLS are examined. We detected an accumulation of activated Tregs in parallel with $CXCL13^+CD4^+$ TIL, which may influence their expansion. We further found that $CXCL13^+CD4^+$ TIL potentially promote TLS formation and are correlated with B cell infiltration and GC maturation at the tumor site. Due to the unique role of $CXCL13^+CD4^+$ TIL shown here, their production of CXCL13, and a significant presence in BC, we designate this $CD4^+$ T_{FH} subpopulation as $T_{FH}X13$ cells.

Results

$CD4^+$ TIL are the principal cellular source of CXCL13 in human BC. Our previous study detected high levels of *CXCL13* transcripts in $CD4^+$ TIL purified from BC (5). These experiments identified a positive association between *CXCL13* and patient disease-free survival or response to chemotherapy, an observation supported by other reports (31–34). Previously, we excluded significant CXCL13 production by breast tumor cells (5); however, this earlier work did not specifically address whether FDC in the GC of BC-associated TLS were also key CXCL13 producers, as reported for secondary lymphoid organs (15) and human lung tumor–associated TLS (35).

The present study explored the significance of CXCL13 expression by $CD4^+$ TIL and FDC from human BC using several approaches. A retrospective BC cohort (patient data in Supplemental Table 1; supplemental material available online with this article; https://doi.org/10.1172/jci.insight.91487DS1) was evaluated to determine the prognostic values for CXCL13 and FDC. Tumors were equally divided based on high, intermediate, and low *CXCL13* gene expression, which stratified patients into groups with significant differences in disease-free and overall survival, either for the entire cohort or the chemotherapy-treated subgroup (Figure 1A and Supplemental Figure 1A). Multivariate Cox analysis shows *CXCL13* is an independent prognostic factor in BC (Supplemental Table 1). The size of this dataset is too small to provide statistically significant analyses of the 4 BC molecular subtypes (Luminal A, Luminal B, $HER2^+$, and triple negative [TN]); however, when low CXCL13–expressing Luminal A tumors are excluded, the *P* values for both disease-free and overall survival are similarly significant. Alternatively, FDC positivity (using IHC-stained tissue sections from this series scored for a $CD23^{hi}$ network; data not shown) does not predict significant differences in either disease-free or overall survival (Figure 1A and Supplemental Figure 1A), suggesting that FDC are unlikely a major source of CXCL13 in BC. Analysis of human BC TCGA RNA sequencing data (TCGA Research Network: http://cancergenome.nih.gov) supports this conclusion by showing that T, B, or T_{FH} cell marker genes are better correlated with *CXCL13* than FDC marker genes

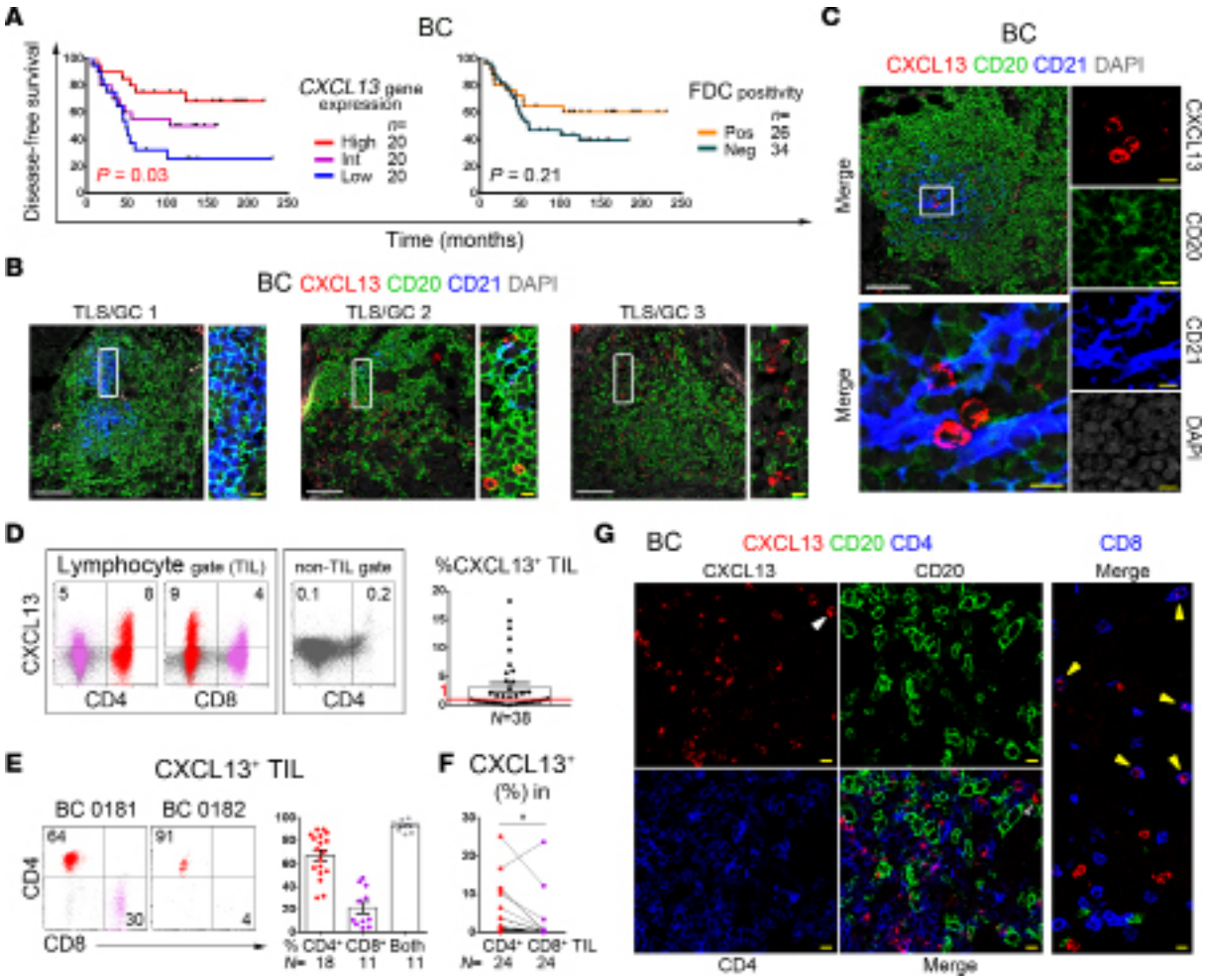


Figure 1. CXCL13 is principally produced by CD4⁺ tumor-infiltrating lymphocytes (TIL) in human breast cancer (BC). (**A**) Kaplan-Meier analysis of disease-free survival for 60 BC patients stratified on *CXCL13* gene expression (qPCR) or FDC network positivity (CD23^{hi} IHC staining). (**B** and **C**) Immunofluorescence (IF) staining of representative BC tissue sections showing CXCL13⁺ TIL (red), CD20⁺ B-TIL (green), and CD21^{hi} FDC (blue) expression in tertiary lymphoid structures (TLS) containing germinal centers (GC); the zoomed areas (right) are defined by white boxes. In some images, the contrast was enhanced by turning down DAPI (gray) intensity. White and yellow scale bars: 100 μm and 10 μm, respectively (**B**, **C**, and **G**). (**D**) Flow cytometric analysis showing CXCL13 expression in a representative fresh BC homogenate (dot plots) or as the % CXCL13⁺ TIL within the lymphocyte gate for 38 BC (graph). (**E**) Relative proportions of CD4⁺ or CD8⁺ T cells in CXCL13⁺ TIL shown for 2 representative BC (dot plots) or for 11–18 BC patients (bar graph). (**F**) % CXCL13⁺ in CD4⁺ and CD8⁺ TIL pairs from 24 BC patients; paired 2-tailed student *t* test. **P* < 0.05, ***P* < 0.01, ****P* < 0.001, *****P* < 0.0001. (**G**) IF staining of representative BC tissue sections showing CXCL13⁺ (red), CD20⁺ (green), and either CD4⁺ or CD8⁺ (blue) TIL; arrows indicate CXCL13⁺CD4⁻ (white) or CXCL13⁺CD8⁺ (yellow) TIL.

for all BC subtypes (Supplemental Table 2). CXCL13 protein expression by FDC was further explored using confocal microscopy to examine four BCs containing multiple TLS. Small CXCL13⁺ cells (likely lymphocytes) and FDC (CD21^{hi} network; detected only in TLS) were not colocalized in these tumors (Figure 1, B and C, and Supplemental Figure 1, B and C). Tonsils have a dense FDC network so the distinction is less obvious; however, the majority of CXCL13⁺ tonsillar cells are CD21⁻ lymphocytes in and around GC-resident FDC (Supplemental Figure 1D). Confirming our previous observation that breast tumor cells are not CXCL13 producers (5), no significant positive (and some negative) correlations between *CXCL13* and tumor cell marker genes were observed (Supplemental Table 2).

Our previous flow cytometric analysis of BC determined that CXCL13 protein expression was enriched in CD3⁺CD4⁺ T- but not B- or NK-TIL (5); however, these data were from a limited number of tumors. This present study examined CXCL13 expression in a larger number of fresh BC (n = 38; < 2-hour surgical specimens were rapidly analyzed by flow cytometry with no stimulation; patient data in Supplemental Table 3; ref. 36). The chemokine was principally detected in the lymphocyte gate with > 1% CXCL13⁺ TIL present in the 20 of 38 (53%) BC examined (Figure 1D and Supplemental Figure 1E [gating strategies]).

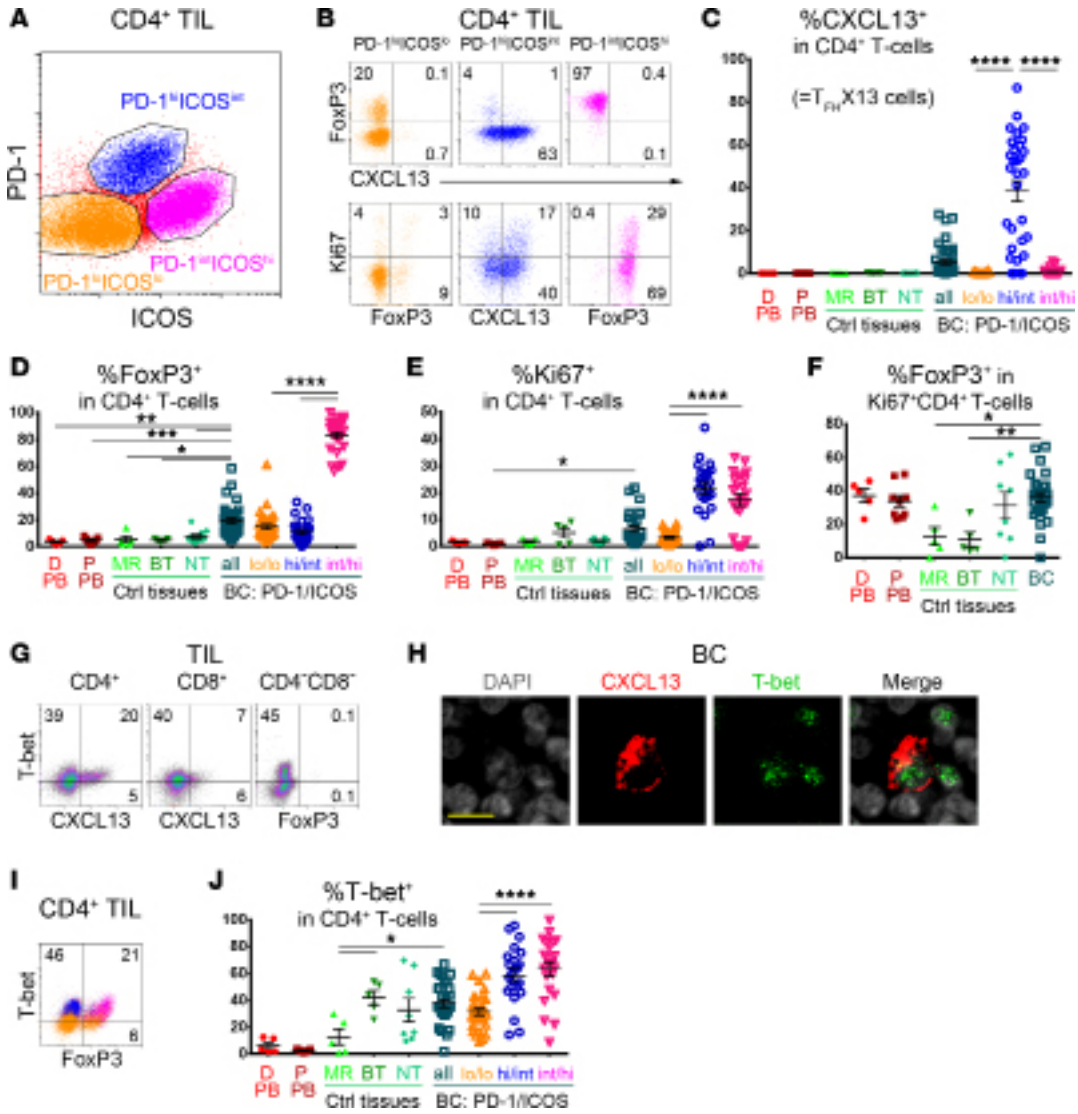


Figure 2. PD-1 and ICOS expression defines 3 CD4⁺ tumor-infiltrating lymphocyte (TIL) subpopulations in human breast cancer (BC). (**A**) Flow cytometric analysis showing PD-1^{lo}ICOS^{lo} (orange), PD-1^{hi}ICOS^{int} (blue; contains T_{FH}X13), and PD-1^{int}ICOS^{hi} (magenta; principally Tregs) CD4⁺ TIL subpopulations in fresh BC tissue homogenates. (**B**) CXCL13, FoxP3, and Ki67 expression in the 3 subpopulations shown in **A**. (**C–E**, **J**) Percentage (flow cytometric analysis) of CXCL13⁺ (**C**), FoxP3⁺ (**D**), Ki67⁺ (**E**), and T-bet⁺ (**J**) CD4⁺ T cells in: healthy donor peripheral blood (D-PB; n = 5), BC patient PB (P-PB; n = 9), mammary reduction tissues (MR; n = 5), benign breast tumors (BT; n = 5), nonadjacent nontumor breast tissue from BC (NT; n = 8–10), and BC tissue (n = 28–38). (**F**) % FoxP3⁺ in Ki67⁺CD4⁺ T cells from the samples in **C**. (**C–F**, **J**) One-way ANOVA followed by Tukey's test. The PD-1/ICOS–defined CD4⁺ TIL subpopulations, and all other samples were independently compared. (**G**) Flow cytometric analysis of CXCL13 and T-bet expression in CD4⁺ and CD8⁺ TIL. T-bet positivity was defined by the distinct populations detected in the CD4⁻CD8⁻ TIL gate. (**H**) Immunofluorescence (IF) staining of CXCL13⁺ TIL (red), T-bet⁺ TIL (green), and DAPI (gray). Yellow scale bar: 10 μm. (**I**) Flow cytometric analysis of T-bet and FoxP3 expression in CD4⁺ TIL. *P < 0.05, **P < 0.01, ***P < 0.001, ****P < 0.0001.

Consistent with our previous observations, CXCL13⁺ TIL were principally in the CD3⁺ T cell compartment (Supplemental Figure 1F), including CD4⁺ but interestingly also in some CD8⁺ TIL (the latter at lower intensities; Figure 1, D and E). The percentage of CXCL13⁺ TIL within the CD4⁺ subpopulation is significantly higher than in the CD8⁺ subpopulation (Figure 1F and Supplemental Figure 1G). Examination of BC tissues using confocal microscopy validated these data, showing that CXCL13⁺ TIL are principally CD3⁺CD4⁺ with scattered CD3⁺CD8⁺ (Figure 1G and Supplemental Figure 1H).

Our earlier work determined that CD4⁺ TIL with a T_{FH} cell phenotype (PD-1^{hi}CD200^{hi}) were specifically associated with CXCL13 expression and expanded in highly infiltrated BC (5). The data in Figure 1 validate the CD4⁺ TIL compartment as the principal source of CXCL13 in human BC and show that their frequencies vary between individual tumors. The data presented throughout this study support a T_{FH} cell nature for CXCL13⁺CD4⁺ TIL, and therefore, for simplicity, we identify them as T_{FH}X13 cells.

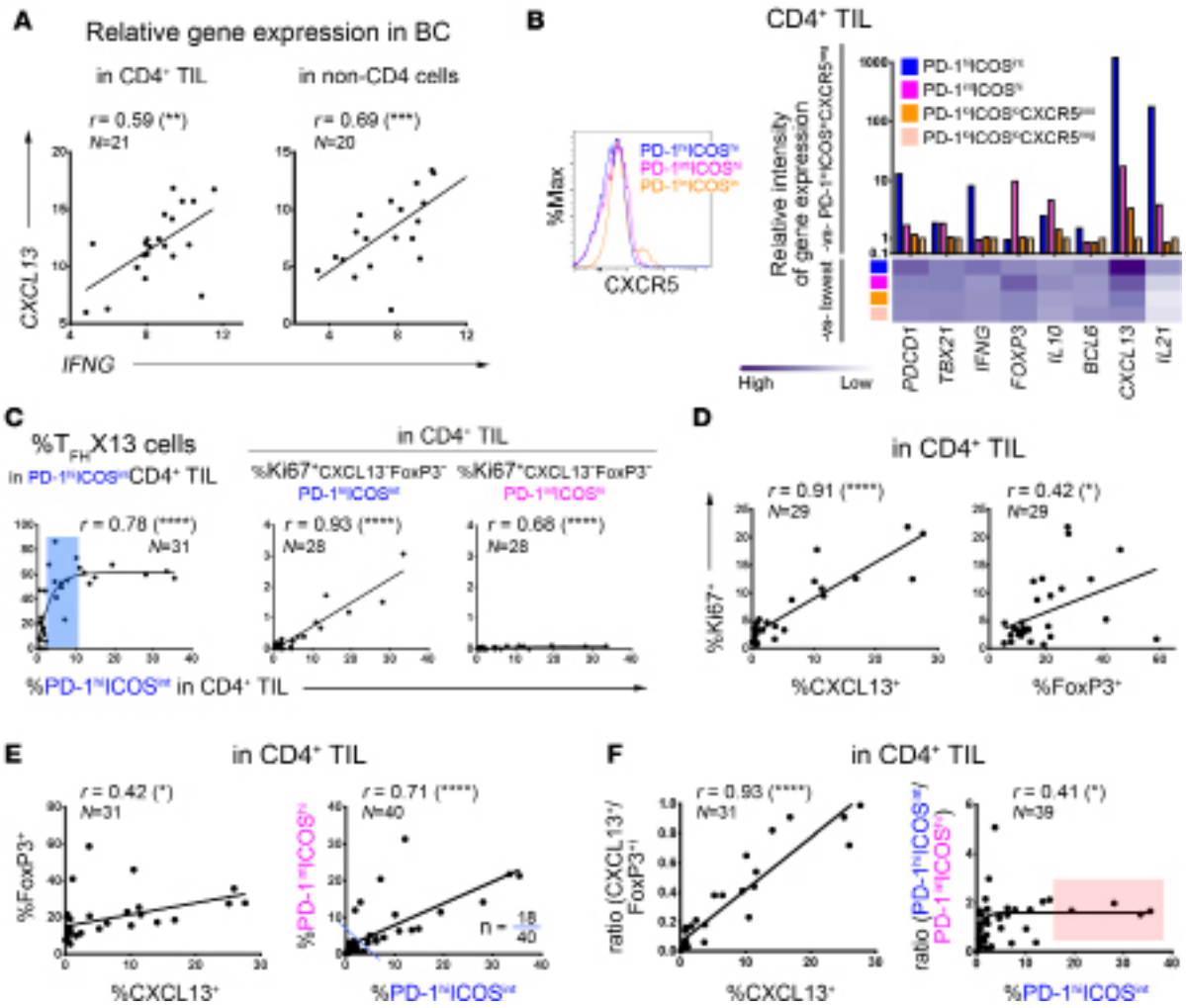


Figure 3. Relationships between the PD-1/ICOS–defined CD4⁺ tumor-infiltrating lymphocyte (TIL) subpopulations in human breast cancer (BC). (**A**) Correlation between *CXCL13* and *IFNG* gene expression (qPCR) in RNA extracted from purified CD4⁺ TIL or CD4-depleted fresh BC homogenates. (**B**) PD-1/ICOS–defined CD4⁺ TIL subpopulations: CXCR5 positivity (flow cytometry; histograms); marker gene expression in purified subpopulations (qPCR data; graph) from an extensively infiltrated BC. (**C–F**) Correlations based on flow cytometric analysis to determine the percentage of positive cells in fresh BC homogenates (*n* = indicated in each graph): (**C**) between T_{FH}X13 containing PD-1^{hi}ICOS^{int}CD4⁺ TIL and specific CD4⁺ TIL subpopulations (as indicated; blue zone represents ; (**D**) between Ki67 and CXCL13 or FoxP3 expression in CD4⁺ TIL; (**E**) between (left) CXCL13 and FoxP3 and (right) PD-1^{hi}ICOS^{int} and PD-1^{int}ICOS^{hi} in CD4⁺ TIL (18 of 40 BC contain significant levels of both subpopulations); and (**F**) between (left) CXCL13 and the CXCL13⁺/FoxP3⁺ ratio, and (right) PD-1^{hi}ICOS^{int} and the PD-1^{hi}ICOS^{int}/PD-1^{int}ICOS^{hi} ratio in CD4⁺ TIL. **P* < 0.05, ***P* < 0.01, ****P* < 0.001, *****P* < 0.0001.

PD-1^{hi}ICOS^{int} and PD-1^{int}ICOS^{hi} CD4⁺ TIL are activated subpopulations containing T_{FH}X13 and Tregs, respectively. Increased expression of *FOXP3*, T_{FH} and Th1 (but not Th2 or Th17) genes was previously detected in our analysis of purified CD4⁺ TIL from highly infiltrated BC (5). The relationship and balance between the different CD4⁺ TIL subpopulations (Th1, Tregs, and T_{FH}/T_{FH}X13 cells) could provide insight on differences in the BC microenvironment with potential clinical relevance. A series of fresh BC tissues (*n* = 42; Supplemental Table 3) were examined for CXCL13 expression, together with consensus T_{FH} markers (PD-1, CXCR5, and ICOS; determined in studies of human tonsils; ref. 23), Th1 (T-bet⁺), and Treg (FOXP3^{hi}) lineage–specifying transcription factors (37) and the proliferation marker Ki67 (Figure 2 and Supplemental Figure 2). Peripheral blood (PB) from healthy donors (D-PB) and BC patients (P-PB) (Supplemental Table 3), mammary reduction tissues, benign breast tumors, and nonadjacent nontumor BC tissues were used as controls.

An unexpected but interesting initial observation was the segregation of CD4⁺ TIL into 3 distinct subpopulations: PD-1^{lo}ICOS^{lo}, PD-1^{hi}ICOS^{int}, and PD-1^{int}ICOS^{hi} TIL (Figure 2A) based on these 2 markers alone. The PD-1^{hi}ICOS^{int} and PD-1^{int}ICOS^{hi} subpopulations are enriched in BC, with negligible levels detected in

other breast tissues (Supplemental Figure 2A). T_{FH}X13 cells are uniquely found in PD-1^{hi}ICOS^{int} TIL, while PD-1^{int}ICOS^{hi} TIL are principally FOXP3^{hi}CD25^{hi} Tregs (Figure 2, B–D, and Supplemental Figure 2B). Small proportions of FOXP3$^{+/-}$CD25^{+} TIL are also detected in the other 2 subpopulations, likely reflecting activated T cells and/or uncommitted/resting Tregs (38, 39). Both PD-1^{hi}ICOS^{int} and PD-1^{int}ICOS^{hi} TIL contain more proliferative (Ki67^{+}) cells than PD-1^{lo}ICOS^{lo} TIL (Figure 2, B and E), suggesting that these subpopulations are more activated. Interestingly, the proportion of FOXP3^{+} cells within the Ki67^{+}CD4^{+} subpopulation is lower in mammary reduction tissues and benign breast tumors compared with BC (Figure 2F). The majority of CXCR5^{+} cells were in the PD-1^{lo}ICOS^{lo} TIL (Supplemental Figure 2C), with a low frequency of conventional T_{FH} cells (PD-1^{hi}CXCR5^{hi}ICOS^{hi}) detected in BC.

T_{FH}X13 TIL (>1% of total CD4^{+}) were detectable in 20 of 38 (53%) BC (Supplemental Figure 2D), while FOXP3^{+} TIL (>5%) were present in 33 of 33 (100%) BC. No CXCL13 (<1%) and only low FOXP3 expression was measurable in D-PB/P-PB and nonmalignant breast tissues (Figure 2, C and D). High proportions (>5%) of T_{FH}X13 TIL are most frequently detected in histological grade 3 tumors, in contrast with FOXP3^{+} TIL found at high levels (>15%) in both grade 2 and grade 3 BC (Supplemental Figure 2E). High *CXCL13* gene expression is associated with improved survival independent of tumor grade (Supplemental Figure 2F). T-bet expression was not sufficient to differentiate Th1 from either T_{FH}X13 or Treg TIL, since its expression was significant in both PD-1^{hi}ICOS^{int}CXCL13^{+} and PD-1^{int}ICOS^{hi}FOXP3^{hi} TIL (Figure 2, G–I). An interesting difference was seen between mammary reduction tissues and benign breast tumors, with the latter containing higher proportions of T-bet^{+} but not FOXP3^{+}CD4^{+} T cells (Figure 2, D and J).

An increase in PD-1^{hi}ICOS^{int} TIL is linked with T_{FH}X13 TIL expansion accompanied by Treg accumulation. IFNγ protein expression was used as a prototypic Th1 marker to further analyze BC tissues for the broad T-bet staining observed in CD4^{+} TIL. IFNγ^{+} cells are readily detectable in BC; however, its expression in T cells is sporadic, with the majority of IFNγ^{+} cells negative for the markers T-bet, CD3, and CD8 (Supplemental Figure 3, A–C). IFNγ^{+}T-bet^{-} cells are principally resident in the stroma (n = 9) and were detected in all tumors examined, including TIL$^{lo/-}$ BC. CXCL13^{+} TIL are abundant in some BC tumor beds but are rarely found in the proximity of IFNγ^{+} cells. Despite the low sensitivity of detection for IFNγ protein in T cells, *IFNG* transcripts correlated positively with *CXCL13* in both CD4^{+} and CD4-depleted fresh BC homogenates (Figure 3A) (5). We also examined gene expression in CD4^{+} TIL subpopulations sorted on PD-1 and ICOS, with the CXCR5-enriched PD-1^{lo}ICOS^{lo} TIL further subdivided into CXCR5^{+} and CXCR5^{-} (Figure 3B). The T_{FH} cell marker genes *BCL6*, *CXCL13*, and *IL21*, along with *IFNG*, were all enriched in PD-1^{hi}ICOS^{int} TIL, suggesting the presence of effector cells (including T_{FH} cells) in this CD4^{+} TIL subpopulation. *PCDC1* (PD-1), *TBX21* (T-bet), and *FOXP3* gene expression mirrored the flow cytometry protein data (Figure 2).

The broad range of T_{FH}X13 cell frequencies in PD-1^{hi}ICOS^{int} TIL detected in different tumors (Figure 2C) suggests that acquisition of CXCL13 expression could be progressive. Thus, as PD-1^{hi}ICOS^{int} TIL accumulate in the tumor (Figure 3C, left graph), T_{FH}X13 TIL first rapidly increase, followed by a heterogeneous stage (blue zone) before finally reaching a dominant equilibrium. This directly contrasts with FOXP3^{+} cell accumulation in the same subpopulation (Supplemental Figure 3D). In line with the enrichment of other cytokines (*IFNG* and *IL21*), we detected some Ki67^{+}, T-bet^{+}, or BCL6^{+} cells that were negative for both FOXP3 and CXCL13 in PD-1^{hi}ICOS^{int} TIL (Supplemental Figure 3E). As this subpopulation accumulates, the global extent of Ki67^{+}FOXP3^{-}CXCL13^{-}PD-1^{hi}ICOS^{int}CD4^{+} TIL increases linearly, in contrast with the limited accrual of Ki67^{+}CXCL13^{-}FOXP3^{-}PD-1^{int}ICOS^{hi}CD4^{+} TIL (Figure 3C, right graphs). These data suggest that the PD-1^{hi}ICOS^{int} subpopulation (in contrast with the PD-1^{int}ICOS^{hi} subpopulation) contains significant numbers of effector cells other than T_{FH}X13 TIL. T_{FH}X13 cells appear to specifically differentiate in a substantial number of BC, where they constitute an important component of effector CD4^{+} TIL.

Globally, proliferation was better correlated with CXCL13^{+} than FOXP3^{+} CD4^{+} TIL (Figure 3D), suggesting that CXCL13 is more consistently expressed by activated TIL. A modest positive correlation was observed between CXCL13 and FOXP3 expression, which improved significantly by comparing PD-1^{hi}ICOS^{int} (effector including T_{FH}X13) with PD-1^{int}ICOS^{hi} (FOXP3^{hi} Treg) TIL (Figure 3E). Significant proportions of both subpopulations were detected in 18 of 40 (45%) BC analyzed with 4 tumors (10%) containing an unbalanced, high proportion of PD-1^{int}ICOS^{hi} (FOXP3^{hi} Treg) TIL. One interpretation is that, in some tumors, Treg activation and accumulation influences T_{FH}X13 and other effector CD4^{+} TIL responses. Alternatively, T_{FH}X13 TIL accumulation might limit Treg expansion. The latter interpretation is supported by our data that T_{FH}X13 TIL increase linearly, reaching parity with FOXP3^{+}CD4^{+} TIL (Figure 3F, left graph). The proportion of PD-1^{hi}ICOS^{int} effector TIL increases rapidly

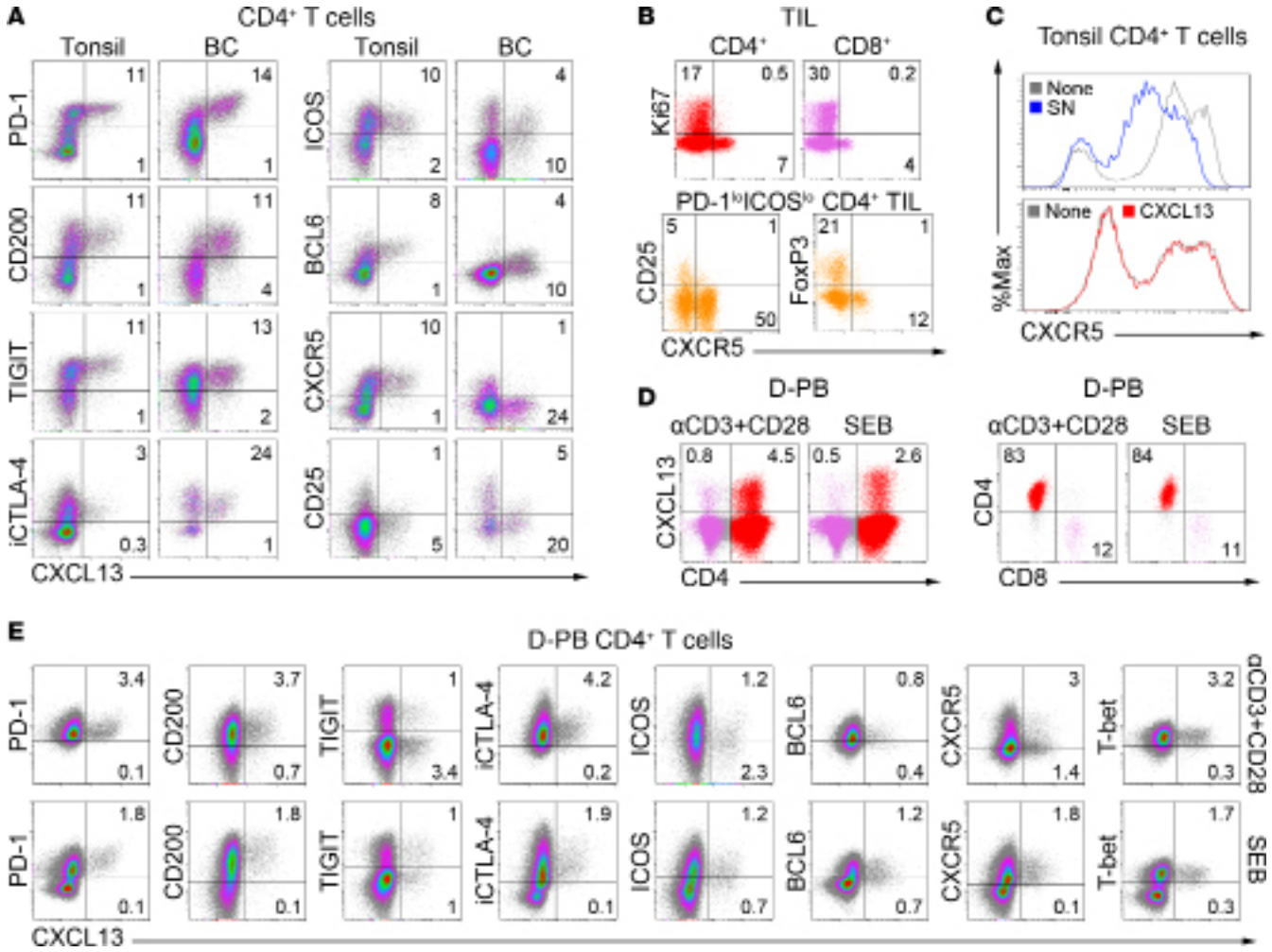


Figure 4. Immunophenotype of breast cancer (BC) $T_{FH}X13$ tumor-infiltrating lymphocytes (TIL) in comparison with their counterparts from blood and tonsils. Flow cytometric analyses showing: (**A**) T_{FH} and Treg/activation marker expression on CXCL13$^+$CD4$^+$ T cells in fresh tissue homogenates from a representative tonsil and BC; (**B**) proliferation and activation markers associated with CXCR5$^+$CD4$^+$ or CXCR5$^+$CD8$^+$ TIL; (**C**) CXCR5 expression on tonsillar CD4$^+$ T cells indicating (top) ± primary tumor supernatant (SN; representative data shown for 3 tonsils using 12 BC SN) and (bottom) ± CXCL13 (representative data shown for 3 tonsils); (**D**) CXCL13 expression after stimulation of healthy donor peripheral blood (D-PB) with αCD3/αCD28 Ab or Staphylococcal enterotoxin B (SEB); and (**E**) expression of the markers in **A** plus T-bet on stimulated D-PB CD4$^+$ T cells.

to 1.8-fold more than PD-1^{int}ICOS^{hi} Treg TIL, but this expansion is stable only in $T_{FH}X13$ TIL-rich BC (≥15% of CD4$^+$ TIL; Figure 3F, red zone, right graph, and Supplemental Figure 3F).

BC $T_{FH}X13$ TIL are phenotypically different from their tonsillar counterparts. The apparent preferential accumulation of $T_{FH}X13$ TIL in the effector CD4$^+$ TIL subpopulation led us to examine their phenotype, differentiation, and function(s) in greater detail. Previously, we ascertained that $T_{FH}X13$ TIL were atypically CXCR5$^-$ (5); therefore, an extended panel of markers was used to compare them with their tonsillar counterparts (Figure 4A). $T_{FH}X13$ cells in both tissues express the highest levels of PD-1, CD200, and TIGIT and are similarly intracellular CTLA-4$^+$ (iCTLA-4$^+$) and CD25^{lo}. Significant differences were detected for ICOS and BCL6 (and CXCR5), with their downregulation detected on BC $T_{FH}X13$ TIL (predominantly CXCR5$^-$) compared with tonsillar $T_{FH}X13$ cells. iCTLA-4 is coexpressed with surface ICOS on global CD4$^+$ TIL (Supplemental Figure 4A). CXCR5$^+$ TIL (both CD4$^+$ and CD8$^+$) proliferate minimally and express low levels of CD25 and FOXP3, suggesting that they are primarily resting cells (Figure 4B). Our previous experiments demonstrated that primary tumor supernatant downregulates CXCR5 expression on D-PB CD4$^+$ T cells (5), an effect we reproduced here using CD4$^+$ T cells purified from tonsils (Figure 4C). This suggests that CXCR5 expression is regulated by factors present in the tumor microenvironment; however, this is not mediated by ligand-induced receptor downregulation, since CXCL13 treatment had no discernable effect.

CXCL13 protein is undetectable in fresh D-PB and P-PB $CD4^+$ T cells (Supplemental Figure 4B) but can be induced by activation (Figure 4D). Similar to BC, $CD4^+$, and $CD8^+$ (to a lesser extent) T cells are the major D-PB populations induced to express CXCL13. In vitro–stimulated $CXCL13^+CD4^+$ T cells acquire a phenotype ($PD\text{-}1^{hi}CD200^{hi}$iCTLA-$4^+ICOS^{int}BCL6^{int}$T-$bet^+$; Figure 4E) similar to BC T_{FH}X13 TIL. A notable difference is the partial preservation of CXCR5 positivity on activated D-PB $CD4^+$ T cells, which is an important distinction with BC $CD4^+$ TIL. Similar to recently activated T cells, CD25 expression is elevated on $CXCL13^+$ cells but lower than on $FOXP3^{hi}$ cells (Supplemental Figure 4C). An unexpected difference was observed in TIGIT expression, with distinct $CXCL13^+TIGIT^{lo}$ and $CXCL13^+TIGIT^{hi}$ subpopulations detected. $CXCL13^+TIGIT^{lo}$ T cells are infrequent in tonsils and BC, tissues where T_{FH}X13 cells may be chronically stimulated and consequently increase their TIGIT expression.

IL2 deprivation is critical for stimulating CXCL13 production but does not affect IFNγ expression in $CD4^+$ T cells. IL2 consumption by Tregs is essential for murine T_{FH} cell development and a subsequent GC response (30). The accumulation of both Tregs and T_{FH}X13 TIL in BC led us to explore the IL2 pathway during T_{FH}X13 cell differentiation. Compared with activation alone, the addition of an IL2-blocking Ab (αIL2) induced significantly higher levels of CXCL13 in D-PB $CD4^+$ T cells (Figure 5A). Differences detected between αCD3/αCD28 and Staphylococcal enterotoxin B (SEB) stimulation are likely due to their ability to activate all or a fraction of $CD4^+$ T cells, respectively. In contrast with TGFβ1 treatment, IL2 deprivation significantly reduces $FOXP3^{hi}$ cells (Supplemental Figure 5A). Increases in $CXCL13^+$ and decreases in $FOXP3^{hi}CD4^+$ T cells are well correlated and αIL2 dose dependent (Supplemental Figure 5B). TGFβ1 was recently shown to be critical for inducing CXCL13 expression in naive $CD4^+$ T cells, with IL2 blockade amplifying this TGFβ1 effect (28). In our experiments, TGFβ1 alone plus SEB activation had no effect on CXCL13 expression but, together with IL2 deprivation, elicited a significant increase (Figure 5B). This effect could also be indirectly triggered by TGFβ1-mediated Treg expansion, which increases IL2 consumption. Our in vitro data nevertheless show that T_{FH}X13 cells can differentiate in an IL2-restricted, TGFβ1-rich microenvironment. Collectively, these data parallel human BC TCGA RNA sequencing data (TCGA Research Network: http://cancergenome.nih.gov) showing a homogenous absence of *IL2* together with high *TGFB1*, low *IFNG*, and broad *CXCL13* gene expression (Figure 5C).

A fraction of induced $CXCL13^+CD4^+$ T cells also produce IFNγ, most apparent in the SEB-activated group (Supplemental Figure 5, C and D). CXCL13 and IFNγ are principally produced by cells expressing the highest levels of PD-1 and ICOS, although the distinct subpopulations detected in $CD4^+$ TIL are not present in D-PB $CD4^+$ T cells activated in vitro (Supplemental Figure 5E). IL2 is a known critical factor for $CD8^+$ T cell IFNγ production; however, our experiments reveal that IL2 deprivation has little impact on IFNγ expression in SEB-activated $CD4^+$ T cells (Figure 5E). Alternatively, TGFβ1 specifically reduces IFNγ expression in the major $FOXP3^{lo}$ subpopulation (Figure 5D), while IL2 deprivation only affects production by the minor $FOXP3^{hi}$ subpopulation (Supplemental Figure 5F). αIL2 treatment of $CD4^+$ TIL did not markedly affect IFNγ expression, despite a net reduction in $FOXP3^+$ cells (Figure 5F and Supplemental Figure 5G).

T_{FH}X13 cells are correlated with B cell maturation in BC TIL. Our data show that the immunosuppressive BC microenvironment can be permissive for T_{FH}X13 TIL accumulation. While CXCL13 expression is strongly associated with improved patient survival, whether T_{FH}X13 TIL mediate this beneficial effect is unknown. To gain insight, we examined CXCR5 expression levels on BC TIL subpopulations, finding that $CXCR5^+$ TIL are primarily B cells, although expression on B-TIL is globally reduced compared with P-PB (Figure 6A and Supplemental Figure 6A [gating strategies]). Interestingly, significant CXCR5 expression on $CD8^+$ T cells was only observed in BC. The best correlation between individual $CXCR5^+$ TIL subpopulations and total $CXCL13^+$ TIL was with $CXCR5^+$ B-TIL (Figure 6B).

Previously, we detected T_{FH} TIL in BC TLS/GCs at the tumor site (5, 25). The majority of T_{FH}X13 TIL are $CXCR5^-$, but small numbers of $CXCR5^{hi}PD\text{-}1^{hi}CXCL13^{+/-}$ TIL (similar to tonsillar GC T_{FH} cells) are found in some tumors, while other T_{FH}X13 TIL-rich BC have none (Figure 6C). For example, 2 BC (MIU-FT-0181 and MIU-FT-0184; Figure 6D) are both T_{FH}X13 TIL rich, but only 0181 (upper plots) has detectable GC T_{FH} TIL. GC B-TIL ($CD38^+IgD^-$, lymphocyte gate) are 2-fold higher in 0181, with a distinct GC phenotype detected only in this tumor. Although proliferating B-TIL in both tumors have an isotype-switched IgD^- phenotype, the majority in 0184 (lower plots) are $CD27^+$ (memory) in contrast with 0181 ($CD27^-$ naive). These data can be interpreted as reflecting ongoing GC B cell maturation in 0181, in contrast with a mature post-GC response in 0184. We more closely examined the B-TIL in the total (viable)

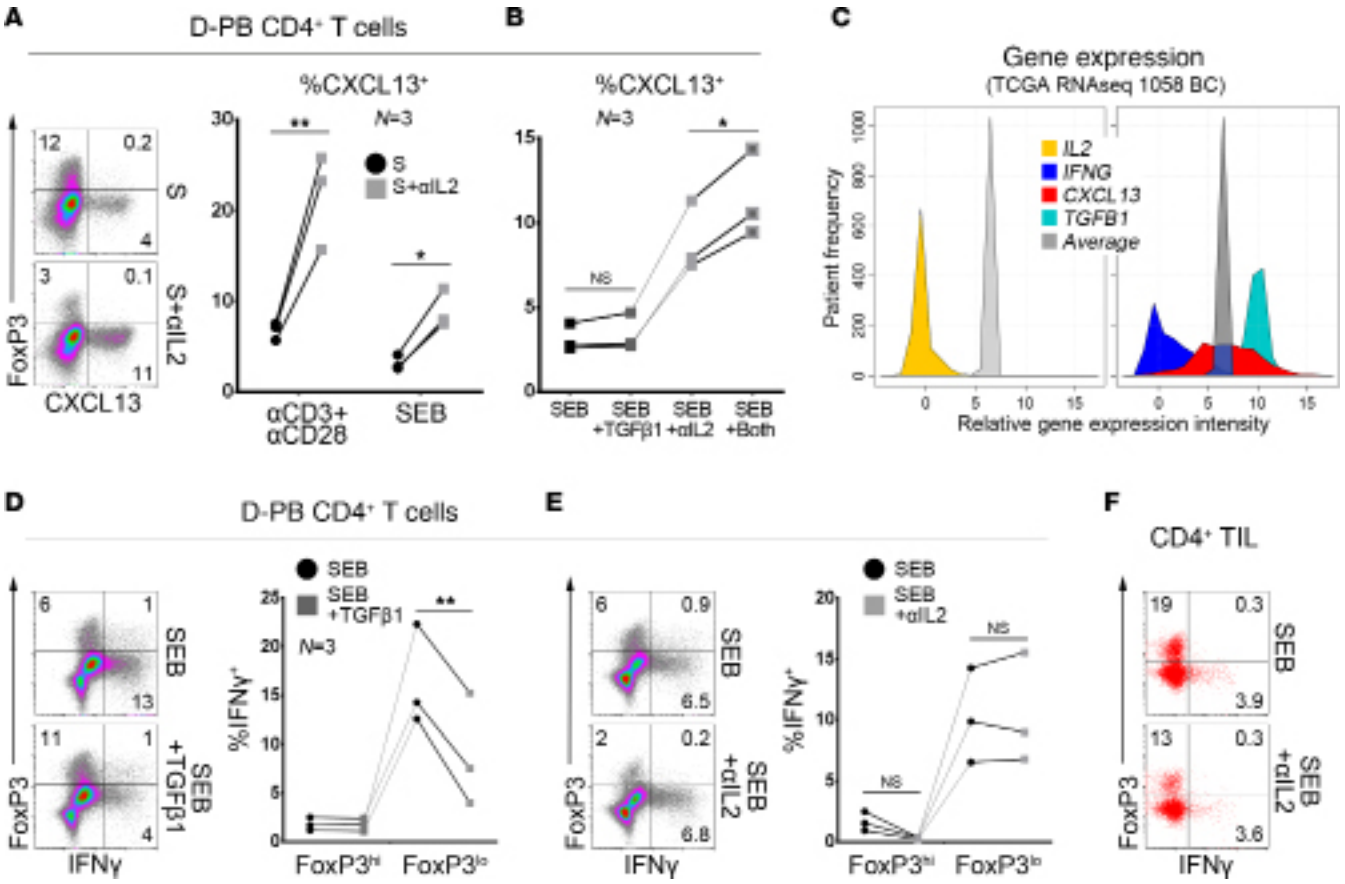


Figure 5. IL2 deprivation promotes CXCL13 production and leads to T_{FH}X13 cell differentiation in vitro. Flow cytometric analysis of CXCL13 expression in stimulated (S; αCD3/αCD28 Ab or Staphylococcal enterotoxin B [SEB]) CD4+ T cells from healthy donor peripheral blood (D-PB): (**A**) ± αIL2 blocking Ab and (**B**) ± αIL2 Ab and/or TGFβ1 (for SEB-stimulated only). (**C**) Expression of the specified genes in TCGA RNA sequencing data from breast cancer (BC) patients; average indicates mean intensity of all genes in this dataset. (**D** and **E**) Flow cytometric analysis of IFNγ expression in FoxP3^{hi} and FoxP3^{lo} subpopulations of SEB-stimulated D-PB CD4+ T cells (**D**) ± TGFβ1 or (**E**) ± αIL2 Ab. (**F**) CD4+ tumor-infiltrating lymphocytes (TIL) ± αIL2 Ab from BC (another tumor is shown in Supplemental Figure 5G). (**A**, **B**, **D**, and **E**) Paired 2-tailed student *t* test. $^{*}P < 0.05$, $^{**}P < 0.01$, $^{***}P < 0.001$, $^{****}P < 0.0001$.

cell gate, which allowed more accurate identification of plasmablasts/plasma cells (PC; CD38^{hi}IgD^{-} or CD38^{hi}CD27$^{int/hi}$), and found that the sum of GC B-TIL plus PC-TIL is similar in both tumors, with proliferating PC 3-fold higher in 0184 than 0181. GC B-TIL (lymphocyte gate) levels appear to reflect rarer tumors containing GC T_{FH} TIL, while total T_{FH}X13 TIL numbers are much more abundant and correlated with GC B-TIL plus PC-TIL (total cell gate; Figure 6E). The proportion of CD27+ memory cells (excluding PC) or PC-TIL within the total proliferating (Ki67+) B-TIL subpopulation (in the lymphocyte or total cell gate, respectively) are perfectly correlated (Figure 6F and Supplemental Figure 6B [gating strategies]), suggesting that they may mature together.

Further investigation into the significance of CXCL13 expression by T_{FH} cells was addressed using gene expression analysis of PD-1 and ICOS-defined tonsillar CD4+ T cell subpopulations (Figure 6G and Supplemental Figure 6C). PD-1^{int}ICOS^{hi} cells are at low frequencies, while the PD-1^{hi}ICOS^{hi} subpopulation appears to be transitioning to PD-1^{hi}ICOS^{hi} (GC T_{FH} phenotype; Supplemental Figure 6D) in tonsils. The tonsillar PD-1^{lo}ICOS^{lo} subpopulation contains a substantial proportion of CD45RA+CCR7+CXCR5^{-} naive cells that are PD-1^{-} (Supplemental Figure 6E; low frequency in BC), so these cells were further separated into memory and naive cells (CD45RA^{-} and CD45RA+, respectively; Figure 6H). Similar to TIL subpopulations, tonsillar PD-1^{hi}ICOS^{hi} CD4+ T cells express the highest levels of *CXCL13* and *IL21* gene transcripts (Figure 6I). *PDCD1* and *IL21* transcripts gradually decrease from PD-1^{hi}ICOS^{hi} to PD-1^{lo}ICOS^{lo} naive cells. *CXCL13* increases are most pronounced in the PD-1^{hi}ICOS^{hi} group, suggesting it might be more specific for tonsillar GC T_{FH} cells than either *PDCD1* or *IL21*. These data support a view that CXCL13 is specific for T_{FH} cell differentiation and thereby important for GC responses.

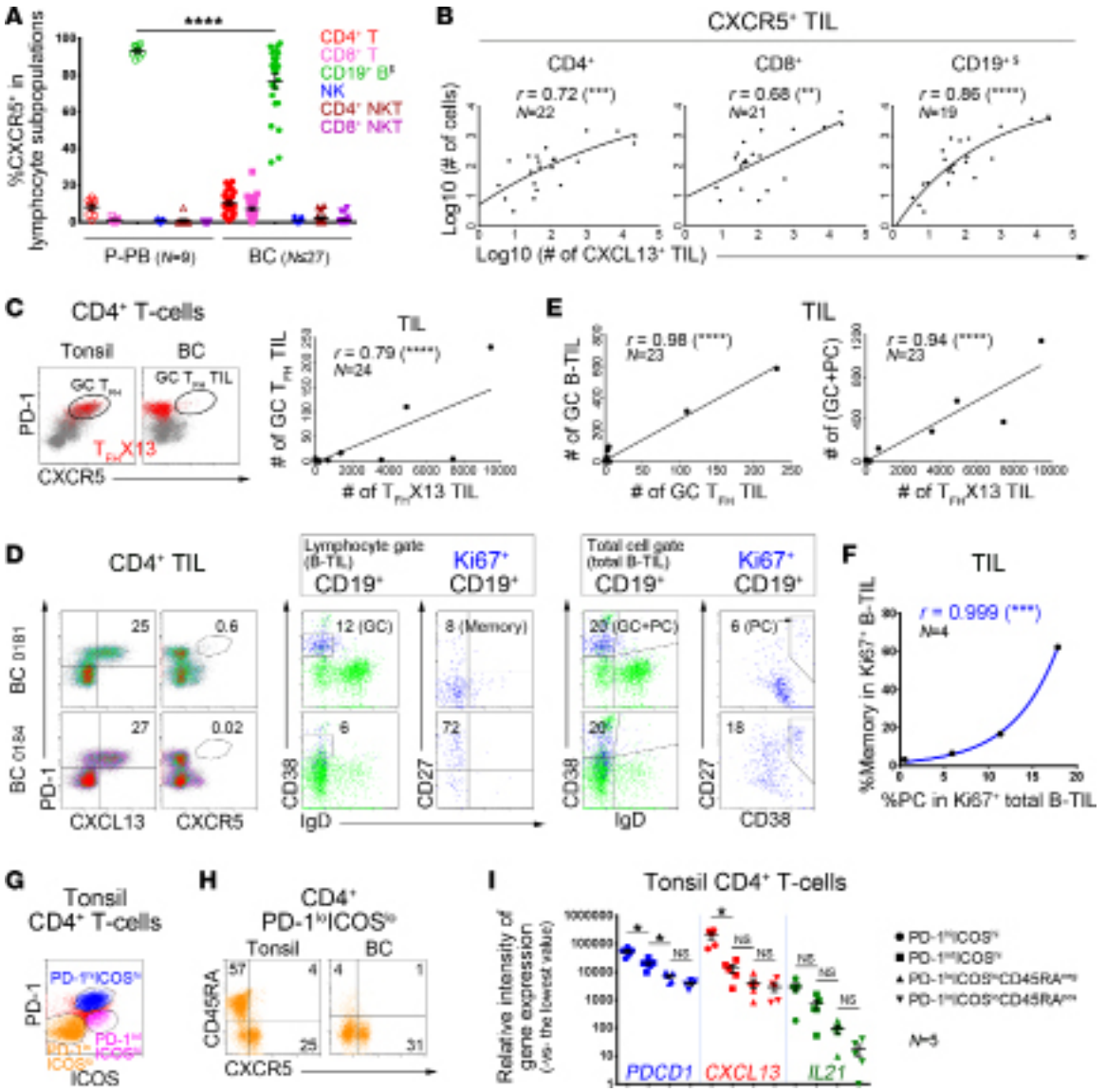


Figure 6. T_{FH}X13 tumor-infiltrating lymphocytes (TIL) in human breast cancer (BC) are correlated with specific B-TIL maturation stages. (**A–H**) Flow cytometric analyses. (**A**) CXCR5 expression in specific lymphocyte subpopulations from patient peripheral blood (P-PB) and BC (n = range 16–27 BC). One-way ANOVA followed by Tukey's test. (**A–D**) Gating strategies are shown in Supplemental Figure 6A; ^{5}B cells were analyzed in the total cell gate. (**B**) Correlation between the number of CXCR5$^+$ cells in specific TIL subpopulations and total CXCL13$^+$ TIL in fresh BC homogenates. (**C**) Germinal center (GC) T_{FH} (PD-1^{hi}CXCR5^{hi}) or T_{FH}X13 (CXCL13$^+$CD4$^+$; red) cells in tonsils and BC (dot plots); correlation between #GC T_{FH} and #T_{FH}X13 BC TIL (graph). (**D**) Equally high T_{FH}X13 TIL responses (left) but distinct proliferating (Ki67$^+$) B-TIL subpopulations (middle and right) in 2 BC. B cell differentiation markers are shown for total CD19$^+$ (green) and Ki67$^+$CD19$^+$ (blue) B-TIL (GC B cells = CD38$^+$IgD$^-$; plasmablasts/plasma cells [PC] = CD38^{hi}IgD$^-$ or CD38^{hi}CD27$^{int/hi}$; CD27 = memory B cell marker). (**E**) Correlation between #GC T_{FH} and #T_{FH}X13 TIL defined in **C** and #B-TIL subpopulations defined in **D**. (**F**) Correlation between % memory cells (excluding PC) in Ki67$^+$ B-TIL (lymphocyte gate) and PC in Ki67$^+$ total B-TIL (total cell gate) from 4 BC with sufficient numbers of Ki67$^+$ B-TIL (gating strategies in Supplemental Figure 6B). (**G**) PD-1/ICOS–defined CD4$^+$ T cell subpopulations from tonsils. (**H**) CD45RA and CXCR5 expression on PD-1^{lo}ICOS^{lo}CD4$^+$ T cells from tonsils and BC. (**I**) Expression of *PDCD1* (PD-1), *CXCL13*, and *IL21* genes (qPCR) in CD4$^+$ T cell subpopulations sorted from 5 tonsils. One-way ANOVA followed by Sidak's test. *P < 0.05, **P < 0.01, ***P < 0.001, ****P < 0.0001.

T_{FH}X13 TIL recruit B-TIL, leading to formation of functional GC at the tumor site. The abundance of CXCL13$^+$ TIL in the tumor bed led us to specifically analyze intratumoral B-TIL (apart from the more abundant stromal B-TIL) using a sizable BC series (n = 51; Supplemental Table 1). Significant numbers (≥ 1%) of intratumoral B-TIL were detected in 16 of 51 BC with lower levels (0%–1%) observed in half of the remaining samples (17 of 35; Figure 7A). Intratumoral B-TIL abundance is significantly correlated with *CXCL13* gene expression. BC with undetectable intratumoral B-TIL (n = 18) are associated with reduced disease-free and overall survival, while high *CXCL13* gene expression consistently predicts better clinical outcomes (Figure 7B and Supplemental Figure 7A).

Confocal microscopy was next used to examine BC tissue for interactions between T_{FH}X13 and B-TIL. A TLS/GC (containing Ki67$^+$CD20$^+$ B-TIL) located at the tumor bed border is shown in Figure 7C. Numerous CXCL13$^+$ TIL are detectable both within the TLS/GC and infiltrating the tumor bed, sometimes next to B-TIL. CXCL13$^+$ TIL are also detectable in proximity to IgA$^+$ or IgG$^+$ (CD20$^-$) PC (Figure 7D). Deep in the tumor bed, where TIL are infrequent, a few B-TIL are seen in close proximity or in direct contact with proliferating CXCL13$^+$ TIL (Figure 7E). These data suggest that CXCL13 secreted by T_{FH}X13 TIL may recruit and guide B-TIL infiltration and migration in the tumor bed.

Rare tumor bed–located B cell follicles were detected in 1 BC (Figure 7F) where dense CD3$^+$ TIL surround the tumor bed and also form a bridge through the middle. Individual B-TIL, as well as compact follicles, are associated with these CD3$^+$ TIL (principally CD4$^+$; Supplemental Figure 7B). Isolated B cell follicles (containing CD4$^+$ TIL) were detected on both sides of the bridge (Figure 7F), with one examined in detail (Figure 7G). A dense CD4$^+$ TIL bridge is opposite this B cell follicle, with a concentration of CXCL13$^+$ TIL (principally CD4$^+$CD8$^-$ T_{FH}X13 TIL) at the border facing the follicle and B-TIL appearing to migrate between the two (Figure 7G, zoomed area 1). Some T_{FH}X13 TIL are located in the follicle (Figure 7G, zoomed area 2), but higher concentrations are visible in small CD4$^+$ TIL aggregates that contain only a few B-TIL (Figure 7G, zoomed area 3). These observations favor the concept that T_{FH}X13 TIL are mediating the formation of a precursor TLS. Further supporting this idea is the obvious correlation between *CXCL13* gene expression and TIL aggregate density (Supplemental Figure 7C). A few CXCL13$^+$CD8$^+$ TIL are at the periphery of the follicle, while a density of proliferating B-TIL (reactive GC) are in the center (Figure 7G). IgG$^+$ (but not IgA$^+$) isotype–switched B-TIL are in the GC (some in direct contact with GC T_{FH}X13 TIL), indicating that functional B cell maturation occurs in the tumor bed. In the IgG-stained section, a small concentration of CXCL13$^+$ TIL are in the follicle, positioned across from higher concentrations of CXCL13$^+$ TIL on the bridge. These CXCL13$^+$ TIL may attract B-TIL recruited to the bridge and direct their migration to the follicle. Together, these data suggest that T_{FH}X13 TIL (potentially in cooperation with CXCL13$^+$CD8$^+$ TIL) play important roles in recruiting and guiding B cell migration in human BC. T_{FH}X13 TIL also appear to promote formation of functional TLS within the tumor, thereby providing a site for GC B-TIL to mature into Ab-secreting PC and memory cells.

Discussion

B cell–mediated humoral immune responses producing high-affinity Ab provide effective life-long protection from reinfection by most viruses. Misdirected humoral responses generate autoreactive memory B cells and auto-Ab characteristic of autoimmune diseases. In humans, their presence has been directly correlated with increased circulating T_{FH} cells and TLS/GC formation in inflamed tissues (40).

In contrast, the functional role(s) of B-TIL are currently poorly understood. Tumor-promoting activities by B cells have been commonly described in animal models (41), whereas most human studies associate B-TIL with positive cancer outcomes (42–44). The latter include dependence on a B-TIL presence for the prognostic value of CD8$^+$ TIL (45), increased CD4$^+$ TIL clonality linked with high B-TIL density (46), and evidence of Ag recognition, somatic hypermutation, and oligoclonality in B-TIL (45).

The B cell chemoattractant, *CXCL13*, has been identified as one of the most robust predictors of improved survival in human cancer (47). Data from murine studies are contradictory with IgA$^+$ PC-mediated immune suppression linked to myofibroblast-derived CXCL13 expression in experimental prostate cancer (48), while direct antitumor effects by CXCL13 were observed in a colon cancer model (6). B cell responses may vary considerably between cancer types, murine models, and individual tumor microenvironments.

The detailed characterization of BC T_{FH}X13 (CXCL13-producing T_{FH}) TIL presented here reveals their presence is tightly linked with B cell maturation at the tumor site. T_{FH}X13 TIL accumulation in BC is characterized by B-TIL and tumor-associated TLS, potentially following a phase of Treg-mediated immunosuppression. The importance of B cell maturation at the tumor site is corroborated by a recent ovarian cancer study linking IgG$^+$ oligoclonal PC surrounding TLS with robust, prognostically favorable CD8$^+$ TIL responses (49).

The role of T_{FH}X13 cells in immunity is unknown, likely due to the lack of an identified equivalent in murine models. We detected CXCL13$^+$ TIL in the tumor bed distant from TLS/GC (5), which led us to explore their T_{FH} cell identity. BC T_{FH}X13 TIL have some phenotypic characteristics similar to T_{FH} cells in secondary lymphoid organs; however, CXCR5, their hallmark receptor (for CXCL13), is absent on most. We found that PD-1^{hi}CXCR5^{hi} GC T_{FH} TIL parallel GC B-TIL, while total T_{FH}X13 TIL, detected in 50% of

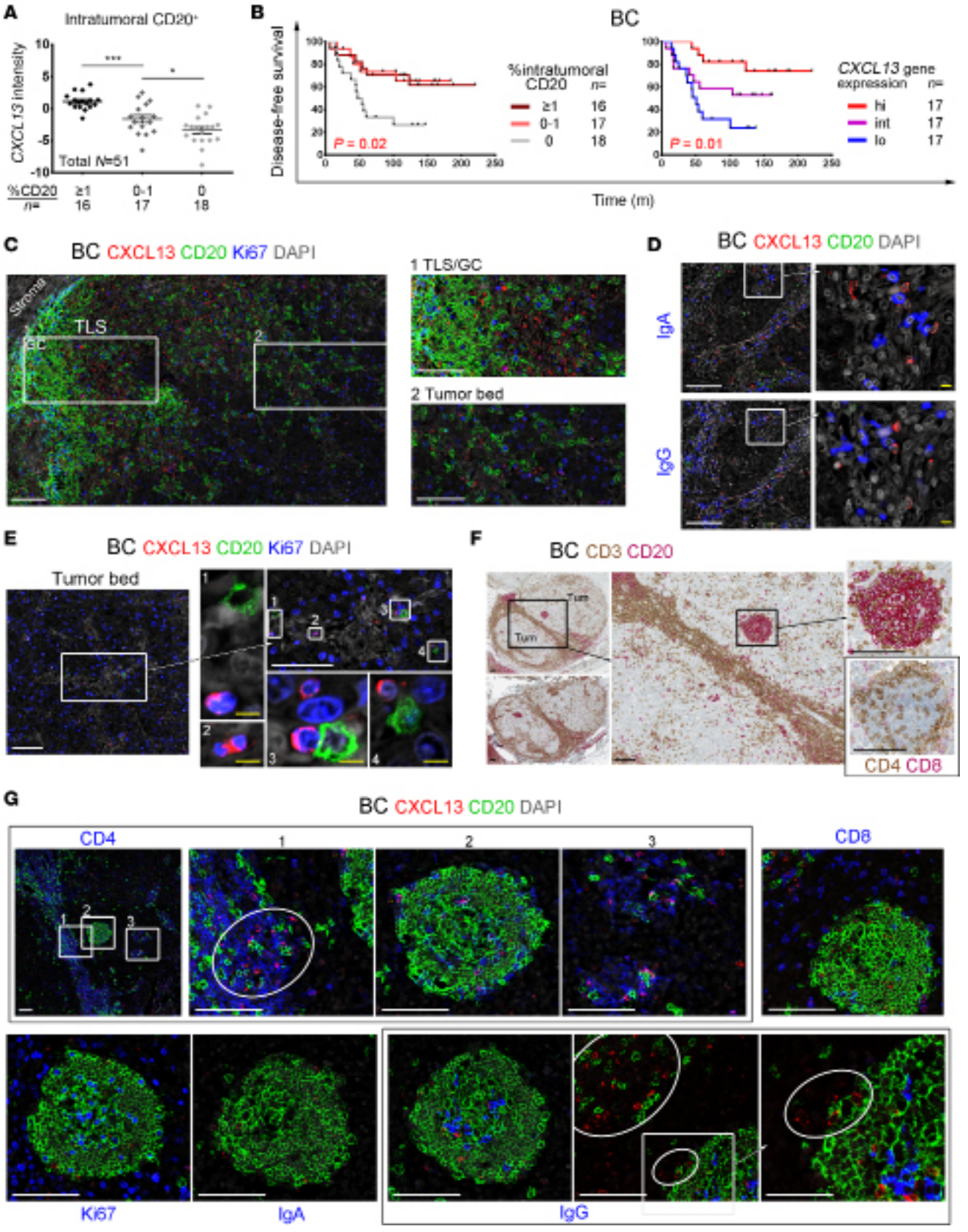


Figure 7. Spatial relationships and interaction between tumor-infiltrating lymphocyte (TIL) subpopulations in human breast cancer–associated (BC-associated) tertiary lymphoid structures (TLS). (**A**) *CXCL13* gene expression in BC samples scored for intratumoral (apart from the more abundant stromal) B-TIL (% CD20⁺ scored on IHC-stained sections by trained pathologists). One-way ANOVA followed by Sidak's test. (**B**) Kaplan-Meier analysis of disease-free survival for 51 BC patients stratified on CD20 (IHC scores defined in **A**) or *CXCL13* gene expression (qPCR). (**C–E**, **G**) Immunofluorescence (IF) staining of BC

tissue sections for: CXCL13$^+$ TIL (red), CD20$^+$ B-TIL (green), and a third marker (blue); the zoomed areas are defined by white boxes. In some images, the contrast was enhanced by turning down DAPI (gray) intensity. White and yellow scale bars: 100 μm and 10 μm, respectively. (**C**) Tumor bed localized CXCL13$^+$ TIL and a TLS containing Ki67$^+$ germinal center (GC) B-TIL. (**D**) CXCL13$^+$ TIL contact CD20$^-$IgA$^+$ or CD20$^-$IgG$^+$ plasmablasts/plasma cells in the tumor bed. (**E**) Deep in the tumor bed, a few B-TIL interact with CXCL13$^+$Ki67$^+$ TIL. (**F**) IHC staining of BC tissue sections for CD3 (brown) and CD20 (red); B-TIL are concentrated in peri- and intratumoral TLS. The spherical tumor bed–localized TLS was IHC stained for CD4 (brown) and CD8 (red); black scale bars: 100 μm. (**G**) The spherical TLS in **F** was also IF stained for CXCL13 and CD20 plus CD4, CD8, Ki67, IgA, or IgG. *$P < 0.05$, **$P < 0.01$, ***$P < 0.001$, ****$P < 0.0001$.

BC, are linearly correlated with GC B-TIL plus PC-TIL. This suggests that, although T_{FH}X13 TIL are not GC restricted, they can mediate T_{FH} cell–related functions. T_{FH}X13 TIL were located in areas that reflect a role in guiding B-TIL migration and thereby likely promoting TLS/GC formation. This observation is supported by the strong correlation between T_{FH}X13 TIL abundance and B-TIL maturation, with proliferating B-TIL ranging from naive (GC) to memory (post-TLS) cells. The association of T_{FH}X13 TIL activities with antigen-specific anti-tumor humoral responses and memory generation may be the causal link between *CXCL13* expression and positive outcomes in BC.

FDC, while present in reactive GC, are not potent CXCL13-producers in BC. Murine studies found that FDC were dispensable for GC B cell development and affinity maturation (50, 51). In humans, full characterization of early events leading to normal GC formation is difficult because tonsils, the most accessible secondary lymphoid tissue, have large B cell follicles and well-formed GC defined by a dense FDC network. The immunosuppressive BC microenvironment may inherently restrict TLS/GC formation, but — under conditions that allow T_{FH}X13 TIL to accumulate — could promote TLS development prior to the arrival and differentiation of FDC.

Our use of PD-1 and ICOS to identify 3 distinct CD4$^+$ TIL subpopulations may facilitate future analyses of Tregs and effector TIL. The PD-1^{int}ICOS^{hi} (iCTLA-4^{hi}) population we identified specifically contain FOXP3^{hi} TIL, which are activated (39), suppressive Tregs, in contrast with FOXP3^{lo}IL17$^+$CD4$^+$ TIL (nonsuppressive) observed in colorectal cancer patients (37). The PD-1^{hi}ICOS^{int} (iCTLA-4^{int}) subpopulation contains all T_{FH}X13 together with various effector TIL. The high proliferation rates of both these subpopulations could reflect an active response to the tumor. Interestingly, lung cancer TIL reactive to clonal neoantigens identified comparable CD4$^+$ phenotypes (52). PD-1^{hi}ICOS^{int} and PD-1^{int}ICOS^{hi} TIL are linearly correlated in 90% of BC, suggesting T_{FH}X13 and activated Treg TIL can expand in parallel. This trend was potentially overlooked by the wide disparity in prognostic values for Treg TIL identified using FOXP3$^+$ IHC alone. Accumulation of T_{FH}X13 TIL appears to slow Treg expansion and may be associated with long-term survival, but elevated numbers were only observed in a small fraction of patients. The ratio between PD-1^{hi}ICOS^{int} and PD-1^{int}ICOS^{hi} TIL may ultimately provide an additional prognostic factor for clinical outcome, but this remains to be confirmed, along with a greater understanding of T_{FH}X13 cell differentiation and function(s) in the tumor microenvironment.

Based on our data, we hypothesize that CXCL13 expression by BC TIL can be influenced by Treg consumption and control of IL2 availability, an effect exhibited during murine T_{FH} cell differentiation and GC responses to influenza infection (30). This idea is further supported by the dramatic increases in CXCL13 we detected in IL2-deprived D-PB CD4$^+$ T cells. The importance of limiting IL2 for T_{FH} cell development was previously demonstrated by DC quenching of IL2 (53), which may require Treg cooperation (54). Taken together, these data suggest that T_{FH}X13 cell differentiation can proceed in the same milieu that drives classical T_{FH} cell differentiation. We also found that *CXCL13* was more specific than *IL21* for tonsillar T_{FH} cells, which links T_{FH}X13 cells more tightly with GC responses. These data are supported by a recent study of HIV infection demonstrating that P-PB CXCL13 levels are an accurate reflection of GC T_{FH} cell activity and the production of broad neutralizing antibodies to HIV (55). Taken together, our data suggest T_{FH}X13 TIL differentiation in BC follows Treg accumulation and that T_{FH}X13 TIL are likely an important T_{FH} cell subset.

IL2 deprivation efficiently reduces FOXP3^{hi} cells without affecting D-PB CD4$^+$ T cell IFNγ expression in vitro, suggesting manipulation of this cytokine could be therapeutically interesting. High-dose IL2 has been successful in a few cancer patients, but it was also shown to expand P-PB ICOS$^+$ Tregs, leading to adverse outcomes (56, 57). In contrast, low-dose IL2 therapy has demonstrated efficacy for treating autoimmune diseases where it functions by increasing Tregs (39), with IL2 neutralization in animal models provoking autoimmunity (58). The generation of CD8$^+$ T cell memory has been shown to also depend on Treg-mediated IL2 reduction (59). Low-dose IL2 treatment further reduces B cell responses in patients with HCV-induced vasculitis without affecting their antiviral immunity (60). A selective decrease in circulating

T_{FH} cells was recently observed in systemic lupus erythematosus patients on low-dose IL2 (61). IL2 restriction may be a mechanism for limiting the proliferation of activated low-affinity T cell clones in inflammatory microenvironments (62), providing a potential explanation for the higher avidity of antigen-specific T_{FH} compared with non–T_{FH} cells (63). Thus, manipulating local IL2 concentrations could be an effective approach for regulating effector and Treg responses in the tumor microenvironment and thereby potentially increasing the efficacy of immunomodulatory therapies.

Th1 cells have been shown to play a direct role both in premalignant immune surveillance (64) and active control of postnatal mammary organogenesis and epithelial rearrangement (65). These data support the increased T-bet we detected in benign breast tumors compared with mammary reduction tissues (in the absence of the increased proportion of $FOXP3^+CD4^+$ T cells seen in invasive tumors). This suggests that Th1 responses may precede Treg accumulation, but as preinvasive lesions progress to BC, they are increasingly offset by Treg activation (PD-1^{int}ICOS^{hi}FOXP3^{hi}). Progressive enrichment of T_{FH}X13 relative to other effector cells in the PD-1^{hi}ICOS^{int} TIL may, however, continue until an equilibrium is reached with Tregs. PD-1 and ICOS (iCTLA-4) expression levels, defining 2 specific $CD4^+$ TIL subpopulations in invasive BC, may reflect the balance between anergy or exhaustion (66) and active suppression (67) that follows activation (68).

T_{FH}X13 TIL were detected in half of our BC cohort and preferentially enriched in high-grade tumors in contrast with FOXP3 (highly expressed in all tumors), suggesting that T_{FH}X13 TIL differentiation follows Treg accumulation. The TGFβ1-mediated activities we observed, including IFNγ downregulation, FOXP3 upregulation, and its synergy with αIL2 for inducing CXCL13, support the view that Treg accumulation importantly precedes T_{FH}X13 TIL development. TGFβ1's effect on CXCL13 expression suggests T_{FH}X13 TIL might be refractory to TGFβ-mediated immune suppression in BC, which is supported by their abundance in the tumor bed. Their persistence in the immunosuppressive tumor microenvironment could explain their ability to attract and guide B-TIL migration through the tumor. Thus, late participation by B-TIL in tumor immunity may be more effective for the generation of antitumor responses (44).

Our data, taken in context with other published research, suggest a scenario for T_{FH}X13 TIL development and its consequences for BC patients: first, IL2 secreted by antigen-activated TIL facilitates Treg proliferation and accumulation at the tumor site and consequently limits IL2 availability for effector TIL; second, in the face of IL2 deprivation, some activated $CD4^+$ TIL increase CXCL13 production, resulting in their differentiation to T_{FH}X13 TIL; third, Treg accumulation increases production of suppressive factors (e.g., TGFβ1), thereby limiting IFNγ^+ Th1 responses without affecting T_{FH}X13 TIL accumulation; and finally, T_{FH}X13 TIL attract and guide B-TIL migration in the tumor microenvironment, resulting in TLS initiation, GC formation, and B-TIL maturation. T_{FH}X13 cells may be an overlooked T_{FH} cell subset whose specialized functions are fundamental for the initiation of GC formation in humans.

In tumors expressing neoantigens, this GC response could generate long-lived antigen-specific memory B cells and PC that contribute to effective antitumor immune responses and help control the outgrowth of residual tumor cells. The balance between T_{FH}X13 and Treg TIL could be a critical factor for the success of this process. The modified BC immune microenvironment that follows T_{FH}X13 TIL accumulation might also permit restoration of Th1 responses. Thus, T_{FH}X13 TIL differentiation as a feedback response to overcome Treg-mediated immune suppression would have the benefit of launching a secondary round of immunity that includes humoral together with cell-mediated immune responses. Our study, identifying T_{FH}X13 cells as a significant portion of PD-1^{hi}ICOS^{int} (iCTLA-4^{int}) effector $CD4^+$ TIL in BC, suggests that they are also potentially important targets for modulation by checkpoint inhibition in cancer.

Methods

Detailed methods and reagents are available in Supplemental Methods.

Patient samples. Tumor and blood samples were obtained from patients who underwent surgical resection for BC or benign breast tumors at the Institut Jules Bordet. Mammary reduction tissues and tonsils were obtained from CHU Saint-Pierre. Patient information is detailed in Supplemental Tables 1 and 3.

Flow cytometry. Tissue fragments from fresh surgical specimens were processed using mechanical dissociation (36) prior to surface or intracellular staining without Golgi-stop reagents. Plate-bound αCD3/αCD28 Ab or SEB were used for in vitro activation in the presence or absence of αIL2 Ab or TGFβ1. Data were acquired on a Navios cytometer (Beckman-Coulter).

IHC and Immunofluorescence (IF). Formalin-fixed paraffin embedded (FFPE) tumor sections were either labeled with αCD20 or αCD23 Ab alone or dual-labeled with αCD3/αCD20 or αCD4/αCD8 by IHC. FFPE tumor and tonsil samples were labeled with αCXCL13 in conjunction with Ab to leukocyte markers before mounting in a DAPI-containing reagent for IF.

Quantitative PCR. FFPE tumor samples were extracted and analyzed using preamplification and commercially available Gene Expression Assays. Sorted tumor and tonsil $CD4^+$ T cell subpopulations were analyzed without preamplification using the primers detailed in ref. 5.

Statistics. Statistical analyses were performed using GraphPad Prism 6 software. Student *t* test and one-way ANOVA were used to calculate *P* values for 2- and multiple-group comparisons, respectively. Data are represented as mean ± SEM, except for paired representations. Linear regression or nonlinear fit methods were applied for correlations when appropriate. *P* values were calculated using correlation coefficients and sample sizes. Log-rank (Mantel-Cox) test was used for calculating *P* values for survival analyses. Multivariate Cox analysis was performed using R software. *P* values <0.05 are considered significant. Degrees of significance: $P < 0.05$ (*), $P < 0.01$ (**), $P < 0.001$ (***), and $P < 0.0001$ (****).

Study approval. The present human studies were reviewed and approved by the Medical Ethics Committee of the Institut Jules Bordet. BC patients and blood donors provided informed consent prior to their participation in the study. Other residual tissues were obtained anonymously and without clinical data.

Author contributions

CGT conceived the research and designed experiments with support from KWG. CGT performed the majority of experiments with support from EM. LB collected clinical data and supervised IHC staining with support from S. Garaud. ADW and DL performed pathological evaluations. CGT and SB performed statistical and public data analyses. S. Garaud provided methodological expertise on IF staining and B cell phenotyping. CGT, EM, GN, LDCV, JNL, and HD performed flow cytometry and cell-sorting experiments. JNL and CN performed the majority of qPCR experiments and IHC staining, respectively. S. Gorely proposed important analysis and data presentation. DL provided patient samples. KWG supervised the research. CGT, EM, and KWG analyzed and interpreted the data. CGT and KWG wrote the paper. All authors provided advice on the final manuscript.

Acknowledgments

We thank Nicolas van Baren, Ligia Craciun, and Arnaud Marchant for critical reading of the manuscript. We thank Gert Van den Eynden, Cinzia Solinas, and Anais Boisson for important practical support. We thank Christos Sotiriou and his lab for providing some cDNA patient samples. This work was supported by grants from the Belgian Fund for Scientific Research (FNRS), Les Amis de l'Institut Bordet, FNRS-Opération Télévie, Plan Cancer of Belgium, Fonds Lambeau-Marteaux, and Fonds J.C. Heuson. Confocal microscopy images were acquired at the Center for Microscopy and Molecular Imaging (CMMI), which is supported by the Walloon Region and the ERDF (Wallonia-Biomed portfolio, 411132-957270). Some results shown here are in part based upon data generated by the TCGA Research Network: http://cancergenome.nih.gov/.

Address correspondence to: Karen Willard-Gallo, Molecular Immunology Unit, Institut Jules Bordet, Université Libre de Bruxelles, 121 Boulevard de Waterloo, B1000 Brussels, Belgium. Phone: 32.2.541.3739; E-mail: kwillard@ulb.ac.be or karen.willard-gallo@bordet.be.

CGT's present address is: Institute for Medical Immunology, Université Libre de Bruxelles, Belgium.

1. Crotty S. A brief history of T cell help to B cells. *Nat Rev Immunol*. 2015;15(3):185–189.
2. Ma CS, Deenick EK, Batten M, Tangye SG. The origins, function, and regulation of T follicular helper cells. *J Exp Med*. 2012;209(7):1241–1253.
3. Ueno H, Banchereau J, Vinuesa CG. Pathophysiology of T follicular helper cells in humans and mice. *Nat Immunol*. 2015;16(2):142–152.
4. Linterman MA, Hill DL. Can follicular helper T cells be targeted to improve vaccine efficacy? *F1000Res*. 2016;5.
5. Gu-Trantien C, et al. $CD4^+$ follicular helper T cell infiltration predicts breast cancer survival. *J Clin Invest*. 2013;123(7):2873–2892.
6. Bindea G, et al. Spatiotemporal dynamics of intratumoral immune cells reveal the immune landscape in human cancer. *Immunity*. 2013;39(4):782–795.
7. van de Pavert SA, et al. Chemokine CXCL13 is essential for lymph node initiation and is induced by retinoic acid and neuronal

stimulation. *Nat Immunol*. 2009;10(11):1193–1199.
8. Jones GW, Jones SA. Ectopic lymphoid follicles: inducible centres for generating antigen-specific immune responses within tissues. *Immunology*. 2016;147(2):141–151.
9. Neyt K, Perros F, GeurtsvanKessel CH, Hammad H, Lambrecht BN. Tertiary lymphoid organs in infection and autoimmunity. *Trends Immunol*. 2012;33(6):297–305.
10. Dieu-Nosjean MC, Giraldo NA, Kaplon H, Germain C, Fridman WH, Sautès-Fridman C. Tertiary lymphoid structures, drivers of the anti-tumor responses in human cancers. *Immunol Rev*. 2016;271(1):260–275.
11. Adachi Y, et al. Distinct germinal center selection at local sites shapes memory B cell response to viral escape. *J Exp Med*. 2015;212(10):1709–1723.
12. Marinkovic T, et al. Interaction of mature CD3+CD4+ T cells with dendritic cells triggers the development of tertiary lymphoid structures in the thyroid. *J Clin Invest*. 2006;116(10):2622–2632.
13. Luther SA, Lopez T, Bai W, Hanahan D, Cyster JG. BLC expression in pancreatic islets causes B cell recruitment and lymphotoxin-dependent lymphoid neogenesis. *Immunity*. 2000;12(5):471–481.
14. Yamamoto K, et al. Anti-CXCL13 antibody can inhibit the formation of gastric lymphoid follicles induced by Helicobacter infection. *Mucosal Immunol*. 2014;7(5):1244–1254.
15. Allen CD, Cyster JG. Follicular dendritic cell networks of primary follicles and germinal centers: phenotype and function. *Semin Immunol*. 2008;20(1):14–25.
16. Katakai T, et al. Organizer-like reticular stromal cell layer common to adult secondary lymphoid organs. *J Immunol*. 2008;181(9):6189–6200.
17. Crotty S. Follicular helper CD4 T cells (TFH). *Annu Rev Immunol*. 2011;29:621–663.
18. Kielczewski JL, Horai R, Jittayasothorn Y, Chan CC, Caspi RR. Tertiary Lymphoid Tissue Forms in Retinas of Mice with Spontaneous Autoimmune Uveitis and Has Consequences on Visual Function. *J Immunol*. 2016;196(3):1013–1025.
19. Kim CH, Lim HW, Kim JR, Rott L, Hillsamer P, Butcher EC. Unique gene expression program of human germinal center T helper cells. *Blood*. 2004;104(7):1952–1960.
20. Rasheed AU, Rahn HP, Sallusto F, Lipp M, Müller G. Follicular B helper T cell activity is confined to CXCR5(hi)ICOS(hi) CD4 T cells and is independent of CD57 expression. *Eur J Immunol*. 2006;36(7):1892–1903.
21. Wang C, Hillsamer P, Kim CH. Phenotype, effector function, and tissue localization of PD-1-expressing human follicular helper T cell subsets. *BMC Immunol*. 2011;12:53.
22. Kroenke MA, et al. Bcl6 and Maf cooperate to instruct human follicular helper CD4 T cell differentiation. *J Immunol*. 2012;188(8):3734–3744.
23. Yu D, Vinuesa CG. The elusive identity of T follicular helper cells. *Trends Immunol*. 2010;31(10):377–383.
24. Chakera A, Bennett SC, Morteau O, Bowness P, Luqmani RA, Cornall RJ. The phenotype of circulating follicular-helper T cells in patients with rheumatoid arthritis defines CD200 as a potential therapeutic target. *Clin Dev Immunol*. 2012;2012:948218.
25. Buisseret L, et al. Tumor-infiltrating lymphocyte composition, organization and PD-1/ PD-L1 expression are linked in breast cancer. *Oncoimmunology*. 2017;6(1):e1257452.
26. Manzo A, et al. Mature antigen-experienced T helper cells synthesize and secrete the B cell chemoattractant CXCL13 in the inflammatory environment of the rheumatoid joint. *Arthritis Rheum*. 2008;58(11):3377–3387.
27. Kobayashi S, et al. A distinct human CD4+ T cell subset that secretes CXCL13 in rheumatoid synovium. *Arthritis Rheum*. 2013;65(12):3063–3072.
28. Kobayashi S, et al. TGF-β induces the differentiation of human CXCL13-producing CD4(+) T cells. *Eur J Immunol*. 2016;46(2):360–371.
29. Ballesteros-Tato A, et al. Interleukin-2 inhibits germinal center formation by limiting T follicular helper cell differentiation. *Immunity*. 2012;36(5):847–856.
30. León B, Bradley JE, Lund FE, Randall TD, Ballesteros-Tato A. FoxP3+ regulatory T cells promote influenza-specific Tfh responses by controlling IL-2 availability. *Nat Commun*. 2014;5:3495.
31. Razis E, et al. Improved outcome of high-risk early HER2 positive breast cancer with high CXCL13-CXCR5 messenger RNA expression. *Clin Breast Cancer*. 2012;12(3):183–193.
32. Song IH, et al. Predictive Value of Tertiary Lymphoid Structures Assessed by High Endothelial Venule Counts in the Neoadjuvant Setting of Triple-Negative Breast Cancer. *Cancer Res Treat*. 2017;49(2):399–407.
33. Bedognetti D, Wang E, Marincola FM. Meta-analysis and metagenes: CXCL-13-driven signature as a robust marker of intratumoral immune response and predictor of breast cancer chemotherapeutic outcome. *Oncoimmunology*. 2014;3:e28727.
34. Stoll G, Enot D, Mlecnik B, Galon J, Zitvogel L, Kroemer G. Immune-related gene signatures predict the outcome of neoadjuvant chemotherapy. *Oncoimmunology*. 2014;3(1):e27884.
35. de Chaisemartin L, et al. Characterization of chemokines and adhesion molecules associated with T cell presence in tertiary lymphoid structures in human lung cancer. *Cancer Res*. 2011;71(20):6391–6399.
36. Garaud S, et al. A simple and rapid protocol to non-enzymatically dissociate fresh human tissues for the analysis of infiltrating lymphocytes. *J Vis Exp*. 2014;(94):52392.
37. Saito T, et al. Two FOXP3(+)CD4(+) T cell subpopulations distinctly control the prognosis of colorectal cancers. *Nat Med*. 2016;22(6):679–684.
38. Takahashi R, Yoshimura A. SOCS1 and regulation of regulatory T cells plasticity. *J Immunol Res*. 2014;2014:943149.
39. Klatzmann D, Abbas AK. The promise of low-dose interleukin-2 therapy for autoimmune and inflammatory diseases. *Nat Rev Immunol*. 2015;15(5):283–294.
40. Ueno H. T follicular helper cells in human autoimmunity. *Curr Opin Immunol*. 2016;43:24–31.
41. Palucka AK, Coussens LM. The Basis of Oncoimmunology. *Cell*. 2016;164(6):1233–1247.
42. Ascierto ML, et al. An immunologic portrait of cancer. *J Transl Med*. 2011;9:146.
43. Germain C, Gnjatic S, Dieu-Nosjean MC. Tertiary Lymphoid Structure-Associated B Cells are Key Players in Anti-Tumor Immunity. *Front Immunol*. 2015;6:67.
44. Guy TV, Terry AM, Bolton HA, Hancock DG, Shklovskaya E, Fazekas de St. Groth B. Pro- and anti-tumour effects of B cells and

antibodies in cancer: a comparison of clinical studies and preclinical models. *Cancer Immunol Immunother*. 2016;65(8):885–896.
45. Nielsen JS, et al. CD20+ tumor-infiltrating lymphocytes have an atypical CD27- memory phenotype and together with CD8+ T cells promote favorable prognosis in ovarian cancer. *Clin Cancer Res*. 2012;18(12):3281–3292.
46. Zhu W, et al. A high density of tertiary lymphoid structure B cells in lung tumors is associated with increased CD4(+) T cell receptor repertoire clonality. *Oncoimmunology*. 2015;4(12):e1051922.
47. Rachidi SM, Qin T, Sun S, Zheng WJ, Li Z. Molecular profiling of multiple human cancers defines an inflammatory cancer-associated molecular pattern and uncovers KPNA2 as a uniform poor prognostic cancer marker. *PLoS ONE*. 2013;8(3):e57911.
48. Shalapour S, et al. Immunosuppressive plasma cells impede T-cell-dependent immunogenic chemotherapy. *Nature*. 2015;521(7550):94–98.
49. Kroeger DR, Milne K, Nelson BH. Tumor-Infiltrating Plasma Cells Are Associated with Tertiary Lymphoid Structures, Cytolytic T-Cell Responses, and Superior Prognosis in Ovarian Cancer. *Clin Cancer Res*. 2016;22(12):3005–3015.
50. Boulianne B, et al. AID-expressing germinal center B cells cluster normally within lymph node follicles in the absence of FDC-M1+ CD35+ follicular dendritic cells but dissipate prematurely. *J Immunol*. 2013;191(9):4521–4530.
51. Yusuf I, et al. Germinal center B cell depletion diminishes CD4+ follicular T helper cells in autoimmune mice. *PLoS ONE*. 2014;9(8):e102791.
52. McGranahan N, et al. Clonal neoantigens elicit T cell immunoreactivity and sensitivity to immune checkpoint blockade. *Science*. 2016;351(6280):1463–1469.
53. Li J, Lu E, Yi T, Cyster JG. EBI2 augments Tfh cell fate by promoting interaction with IL-2-quenching dendritic cells. *Nature*. 2016;533(7601):110–114.
54. Liu Z, Gerner MY, Van Panhuys N, Levine AG, Rudensky AY, Germain RN. Immune homeostasis enforced by co-localized effector and regulatory T cells. *Nature*. 2015;528(7581):225–230.
55. Havenar-Daughton C, et al. CXCL13 is a plasma biomarker of germinal center activity. *Proc Natl Acad Sci USA*. 2016;113(10):2702–2707.
56. Wei S, et al. Interleukin-2 administration alters the CD4+FOXP3+ T-cell pool and tumor trafficking in patients with ovarian carcinoma. *Cancer Res*. 2007;67(15):7487–7494.
57. Sim GC, et al. IL-2 therapy promotes suppressive ICOS+ Treg expansion in melanoma patients. *J Clin Invest*. 2014;124(1):99–110.
58. Setoguchi R, Hori S, Takahashi T, Sakaguchi S. Homeostatic maintenance of natural Foxp3(+) CD25(+) CD4(+) regulatory T cells by interleukin (IL)-2 and induction of autoimmune disease by IL-2 neutralization. *J Exp Med*. 2005;201(5):723–735.
59. de Goër de Herve MG, Jaafoura S, Vallée M, Taoufik Y. FoxP3$^+$ regulatory CD4 T cells control the generation of functional CD8 memory. *Nat Commun*. 2012;3:986.
60. Saadoun D, et al. Regulatory T-cell responses to low-dose interleukin-2 in HCV-induced vasculitis. *N Engl J Med*. 2011;365(22):2067–2077.
61. He J, et al. Low-dose interleukin-2 treatment selectively modulates CD4(+) T cell subsets in patients with systemic lupus erythematosus. *Nat Med*. 2016;22(9):991–993.
62. Voisinne G, Nixon BG, Melbinger A, Gasteiger G, Vergassola M, Altan-Bonnet G. T Cells Integrate Local and Global Cues to Discriminate between Structurally Similar Antigens. *Cell Rep*. 2015;11(8):1208–1219.
63. Fazilleau N, McHeyzer-Williams LJ, Rosen H, McHeyzer-Williams MG. The function of follicular helper T cells is regulated by the strength of T cell antigen receptor binding. *Nat Immunol*. 2009;10(4):375–384.
64. Kang TW, et al. Senescence surveillance of pre-malignant hepatocytes limits liver cancer development. *Nature*. 2011;479(7374):547–551.
65. Plaks V, et al. Adaptive Immune Regulation of Mammary Postnatal Organogenesis. *Dev Cell*. 2015;34(5):493–504.
66. Bengsch B, et al. Bioenergetic Insufficiencies Due to Metabolic Alterations Regulated by the Inhibitory Receptor PD-1 Are an Early Driver of CD8(+) T Cell Exhaustion. *Immunity*. 2016;45(2):358–373.
67. Qureshi OS, et al. Trans-endocytosis of CD80 and CD86: a molecular basis for the cell-extrinsic function of CTLA-4. *Science*. 2011;332(6029):600–603.
68. Fuertes Marraco SA, Neubert NJ, Verdeil G, Speiser DE. Inhibitory Receptors Beyond T Cell Exhaustion. *Front Immunol*. 2015;6:310.